Self-focusing and jet instability of a microswimmer suspension

Levan Jibuti,[1] Ling Qi,[2] Chaouqi Misbah,[2] Walter Zimmermann,[1] Salima Rafaï,[2] and Philippe Peyla[2,*]
[1]*Theoretische Physik I, University of Bayreuth, 95440 Bayreuth, Germany*
[2]*LIPHY-CNRS, University of Grenoble, F-38041 Grenoble, France*
(Received 24 September 2014; published 29 December 2014)

Three-dimensional (3D) numerical simulations are performed on suspensions composed of puller-like microswimmers that are sensitive to light (phototaxis) mimicking microalgae in a Poiseuille flow. Simulations are based on the numerical resolution of the flow equations at low Reynolds numbers discretized on a 3D grid (finite differences). The model reproduces the formation of a central jet of swimmers by self-focusing [Phys. Rev. Lett. **110**, 138106 (2013)] but also predicts an instability of the jet, which leads to its fractionation in clusters. We show that this instability is due to hydrodynamic interactions between microswimmers, which attract each other along the flow direction. This effect was not observed in the experiments conducted on dilute suspensions (i.e., where hydrodynamic interactions are weak). This phenomenon is peculiar for pullers for which collective motions are usually not observed on such a time scale. With this modeling, we hope to pave the way toward a better understanding of concentration techniques of algae (a bottleneck challenge in industrial applications).

DOI: 10.1103/PhysRevE.90.063019 PACS number(s): 47.63.Gd, 47.61.−k, 47.63.mf

I. INTRODUCTION

Microorganism motions are frequently biased by physical or chemical externals fields or gradients. Numerous phenomena in ecology find interpretation based on this kind of property (see, for example, Ref. [1]), and applications in industry expect a lot from the control of biased motions of microorganisms or artificial micropropellers [2]. For example, bacteria suspensions exhibit an instability when the cells' swimming motion is biased due to a gradient of a chemical attractant in a confined channel or in a liquid film [3,4]. Swimmers in a Poiseuille flow exhibit a very rich nonlinear dynamics [5] with swinging and tumbling trajectories, but this dynamics can be strongly affected by an external field. For instance, Kessler [6] studied a suspension of algae that can orient themselves in the gravity field and placed in a vertical Poiseuille flow. The balance of torques exerted on each alga by gravity and flow leads to alga's transverse migration resulting in a narrow central jet (self-focusing) in the case of an upstream flow. Another relevant way to bias swimming is phototaxis. It describes the motion of microswimmers toward a light source [7] thanks to a patched eye embedded in their cytoplasmic membrane. In a preceding study [8], it has been shown that by combining light and a Poiseuille flow, a controlled and reversible self-focusing of a dilute suspension of *Chlamydomonas rheinhardtii* (CR) [7] (a genus green microalga) can be produced. The advantage of light is to control the self-focusing and the remixing, whatever the direction of the flow. If the phenomenon is well understood for individual alga in dilute suspensions, for more concentrated regimes understanding the stability of the jet is largely an open issue. We numerically address this question in the present work.

A model based on that of Zöttl and Stark [5] with a single swimmer allowed us [8] to qualitatively reproduce the self-focusing effect. Here, we reproduce numerically the self-focusing effect of a whole suspension of interacting microswimmers. We also reproduce very well the dynamics of the band width of the jet [8] and its spatial distribution as a function of the flow rate. In addition, we show that the central jet of swimmers produced by the self-focusing effect is unstable and a clustering is predicted by our numerical simulations. This clustering is due to attractive hydrodynamic interactions between oriented algae within the jet. This was not observed experimentally [8] since experiments were performed on dilute suspensions. Collective motions are frequently observed for pushers [9] but not for pullers [10] or marginally and on very long time scales [11]. Here, the combination of light and flow creates an alignment of the swimmers that favors collective behaviors (i.e., due to hydrodynamic interactions) for pullers.

II. MODEL AND NUMERICAL SIMULATIONS

Let us first briefly describe the microswimmer, alga CR [7], and its way of locomotion in order to develop our model. CR is a biflagellated unicellular organism. It is spheroidal in shape with two anterior flagella moving in a back-and-forth movement, producing a jerky breast stroke with a mean swimming speed of $V_0 \sim 50 \pm 20\,\mu$m/s in a waterlike medium [12]. Since the cell radius is $R \sim 5\,\mu$m, Brownian motion is negligible. Therefore, a CR is modeled as a rigid sphere—the body—of radius R transporting a set of volume forces (see Fig. 1), which mimic the flagella and body forces exerted on the fluid [13,14]. This set of forces is an average over one period of the breast stroke [14]. Since each microswimmer taken apart is an isolated body, it must be force free and torque free in the absence of an external field of force (like gravity, for example). A swimmer moves in the fluid due to its own velocity and can also be transported and rotated by the external flow and by the presence of other swimmers through hydrodynamic interactions. Phenomena that are still not very well known can occur at higher concentration, such as flagella synchronization or overlaps of flagella. For the sake of simplicity, we restrict ourselves to the simple swimmer model presented on Fig. 1. Note that CR work at constant force [15] and the model should remain robust at high concentration. In order to model the phototactic property, in the simulations

*philippe.peyla@ujf-grenoble.fr

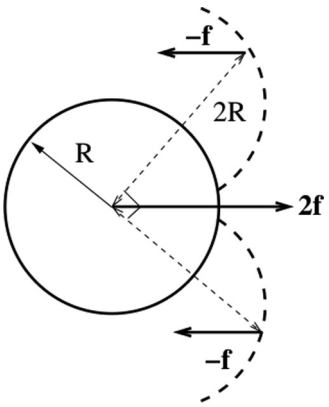

FIG. 1. A *chlamydomonas* model: a spherical bead (the cell body) is bonded to two parallel forces $-\mathbf{f}$ exerted by the flagella (dashed lines) on the fluid and to the force $2\mathbf{f}$ exerted by the body on the fluid. It constitutes a puller [10]. The swimmer must be force free and torque free.

each microswimmer is reoriented toward a given direction (i.e., the direction of the light source) at a given frequency τ^{-1}. Experimentally, τ is typically of about 1 to 2 s [8]. Indeed, the observed phenomena (self-focusing and jet instability) are quite robust, and it appears that time is simply rescaled by τ. Therefore, in the following, we use the dimensionless time t/τ. Of course, if $\tau = 0$, self-focusing is no longer observed. The microswimmers are suspended in a Newtonian fluid of viscosity η_0 in a long channel of length ℓ with a squared section of lateral size $2w$. No-slip conditions are used at the fluid-wall and fluid-particle interfaces. In order to neglect the effect of wall confinement, we choose $w \sim 8.5R$. Note that we chose this confinement value as a compromise since we did not notice quantitative difference with smaller confinements for which computation is much more time-consuming. A pressure gradient is used in order to impose a flow within the channel (i.e., a Poiseuille flow in the absence of particles). The Reynolds number associated with each swimmer is small: $\mathrm{Re} = RV_0/\nu \sim 0.2$ (here numerical velocity is $V_0 \sim 7.10^{-2}\delta$ per time unit, $R = 3\delta$, and the numerical kinematic viscosity is $\nu \sim 1\delta^2$ per time unit). The real Re number is 10^{-4} [8], however we can still neglect inertial effects in our simulations.

The numerical method is the fluid particle dynamics [16], which we have used before for 3D passive or active suspensions [17–19]; for a detailed review and the reliability of the method see Ref. [20]. This method is also known as penalty method in applied mathematics [21]. It consists in replacing solid particles by fluid particles with an inner viscosity η_p much higher than the outer fluid viscosity η_0 ($\eta_p/\eta_0 = 100$). The flow equation is then solved on the entire domain: inside and outside the particles, thus avoiding particle tracking. The translational velocity of the ith particle, $\langle \mathbf{v} \rangle_i$ is obtained by averaging the velocity $\mathbf{v}$ on the volume of that particle. The symbol $\langle \cdot \rangle_i$ represents the average done over the volume of the ith particle. A time step δt is used and at each iteration, the out-of-lattice sphere number i is moved by the quantity $\delta \mathbf{r}_i = \langle \mathbf{v} \rangle_i \delta t$. Then, the viscosity field $\eta(\mathbf{r})$ is recalculated from the new positions of the sphere centers. Time t is simply $t = n\delta t$, where n is the number of time iterations.

Despite the smallness of the Re number, we solve the Navier-Stokes equation (and not the Stokes equation) on the whole domain with a viscosity field $\eta(\mathbf{r})$:

$$\rho \frac{D\mathbf{v}}{Dt} = -\nabla P + \nabla \cdot [\eta(\mathbf{r})(\nabla \mathbf{v} + \nabla \mathbf{v}^t)] + \mathbf{f}, \qquad (1)$$

with the incompressibility constraint ($\nabla \cdot \mathbf{v} = 0$). Here, $D/Dt = \partial/\partial t + \mathbf{v} \cdot \nabla$. Our Navier-Stokes solver works for $0.01 < \mathrm{Re} < 100$ and is very competitive compared to standard Stokes solvers. The volume force $\mathbf{f}$ is the set of forces generated by each swimmer. The resolution of Eq. (1) is then performed using finite differences on a MAC grid [22] with a cubic mesh of size $\delta = 1$. In order to ensure numerical stability, we take $\delta t = 10^{-3}$ [22]. The radius of a swimmer is $R = 3\delta$. The volume forces exerted by each swimmer on the fluid (Fig. 1) are bonded to the spherical particle. Therefore, for the ith particle, we need to know both its translational velocity $\langle \mathbf{v} \rangle_i$ to determine its position and its angular velocity $\langle \mathbf{\Omega} \rangle_i = 1/2 \langle \nabla \times \mathbf{v} \rangle_i$ since it gives its orientation in order to reposition the set of forces belonging to particle i at any time t.

III. RESULTS

A single swimmer, described by the above model, moves in a fluid at rest with a velocity proportional to the force: $v_0 = M f$. The swimmer's mobility M is such that $M = (6\zeta\pi\eta R)^{-1}$, where ζ is a dimensionless parameter that depends on the geometry of the set of forces around the swimmer as well as the confinement due to the walls. For example, with a single force applied on the spherical body, we would have $\zeta = 1$ in an infinite fluid. Here, with the set of three forces bonded to the sphere and with a small confinement ($w/R \sim 8.5$), we found $\zeta \sim 1.14$ in our simulations. This numerical value is very close to the analytical value $\zeta = 32/29 = 1.10$ derived with the Green's function theory [23] in an infinite fluid. The small error of ∼3.5% is mainly due to discretization and of the small confinement. Our numerical modeling thus provides a 3D description of a spherical microswimmer suspension taking into account the full hydrodynamics.

We initially begin the simulation with a suspension of swimmers modeled as described above and homogeneously distributed across a channel with a squared section [see Fig. 2(a)]. The channel length is 100δ and the lateral size is $2w = 50\delta$. The swimmers are initially randomly oriented. A pressure gradient is imposed along the channel and the flow direction is from left to right on the figure and the position of the light source is upstream (i.e., on the left side of the channel). In the absence of particles, we obtain a Poiseuille flow with a maximum velocity at the center: $v_{\max}$. Each swimmer moves with its own velocity and is also transported and rotated by external flow and hydrodynamic interactions with other swimmers. We apply periodic boundary conditions along the flow direction. During that motion each particle is oriented toward the light source at a frequency τ^{-1} but not simultaneously since there is no synchronization among the swimmers. The snapshots in Fig. 2 represent the distribution of swimmers at different times. As shown previously [8], swimmers that reorient themselves regularly upstream are rotated by the flow vorticity and oriented toward the center of

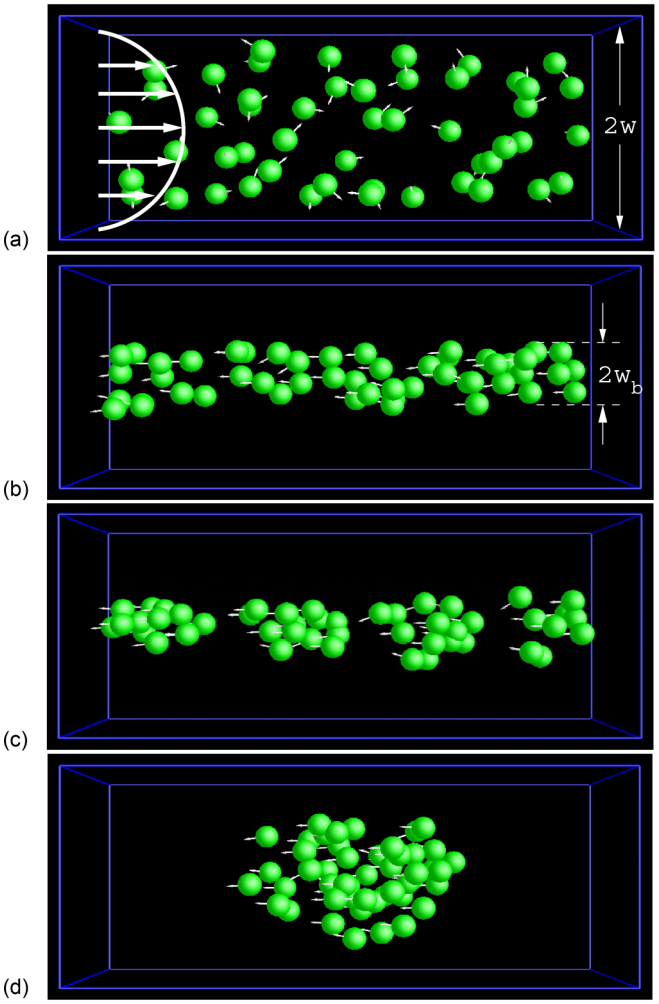

FIG. 2. (Color online) A suspension of 50 swimmers in a channel with a squared cross section of lateral size $2w$. The flow is from left to right ($v_{max}/v_0 = 14$) and the light source's position is upstream (left). (a) Initial state ($t/\tau = 0$) Poiseuille flow is schematically indicated; (b) self-focusing ($t/\tau = 28$) of band width $2w_b$; (c) clustering ($t/\tau = 50$); (d) merging ($t/\tau = 60$).

the flow to which they swim. As shown in Fig. 2(b), this results in a self-focusing effect. In Fig. 3, we plot the lateral half-width w_b of the distribution normalized by w as a function of time. In addition, we alternate the time slots for which reorientations upstream are active and inactive (random reorientation). This simulates a periodic switching of the light with a period chosen to be 20 times longer than the phototactic time τ. Following the self-focusing phase, a redispersion is obtained during the dark phase, showing the reversible character of the phenomenon. The same saw-tooth profile is obtained as in the experiments [8]. We choose flow rates for which flow focusing is obtainable. Note that the dynamics of the band width is not very much affected within this range of flow rates. This time-dependent shape of w_b/w is due to the dynamics of the self-focusing and of the redispersion that are both dominated by the velocity of the cells that migrate across the channel at their own swimming velocity v_0. Therefore, the slope of the saw-tooth profile is proportional to v_0. We also checked the influence of the flow rate on the self-focusing. By changing

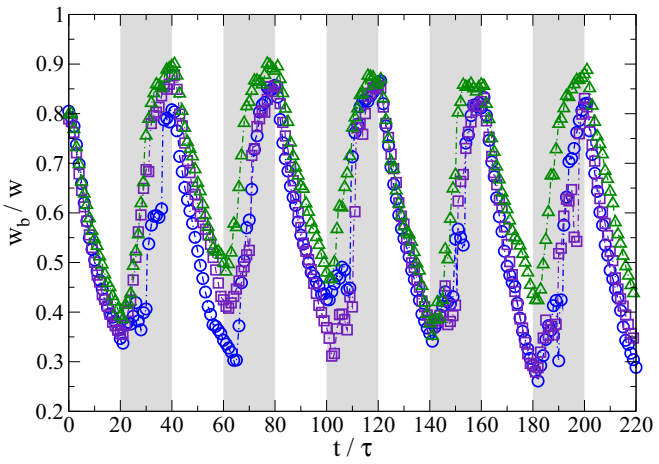

FIG. 3. (Color online) Half width of the jet normalized by the channel half-width w as a function of time when the swimmer suspension is submitted to a light-dark cycle at different flow rates [green: $v_{max}/v_0 = 18$ (triangles), purple: $v_{max}/v_0 = 16$ (squares), blue: $v_{max}/v_0 = 14$ (circles)]. Dark periods are indicated by the gray areas. The self-focusing is observed during the light phases and a redispersion is observed during the dark phases.

the pressure gradient, the maximum velocity of the external flow v_{max} is varied from 0 to 30 times the swimmer velocity v_0. These values are similar to the experimental ones [8]. In inset of Fig. 4, we plot the normalized half band width of the jet as a function of the dimensionless quantity $\dot{\gamma}_{wall}\tau$. A swimmer that migrates toward the center, crossing the flow lines is submitted to a continuous shear rate, which varies from $\dot{\gamma}_{wall}$ (at walls) to 0 (at the center). At low flow rate, when $\dot{\gamma}_{wall}\tau$ is too small, the presence of hydrodynamic diffusion (due to hydrodynamic interactions) screens the swimmer orientation toward the center and self-focusing is inefficient. At high flow rate, a swimmer is oriented in several directions during time τ, it is submitted to successive rotations by the flow

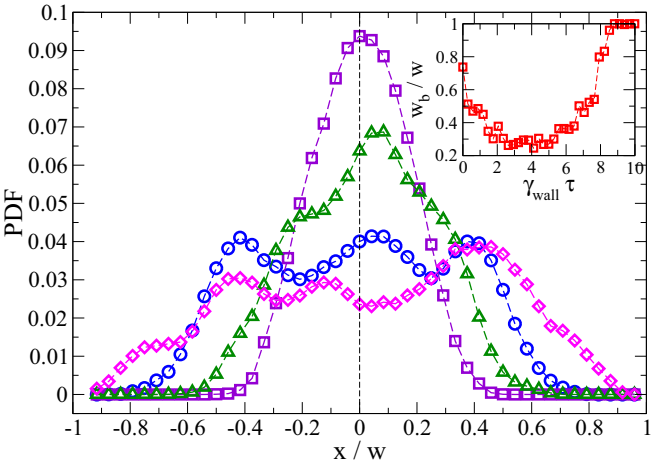

FIG. 4. (Color online) Probability distribution across the channel at several flow rates: $v_{max}/v_0 = 0.5$ (circles), $v_{max}/v_0 = 14$ (squares), $v_{max}/v_0 = 22$ (triangles), $v_{max}/v_0 = 28$ (diamonds). Inset: Half width of the jet (w_b) normalized by the channel half-width w as a function of $\dot{\gamma}_{wall}\tau$ at $t/\tau = 30$.

depending on its distance to the center in the channel and again self-focusing becomes inefficient. For intermediate flow rates (i.e., $2 \lesssim \dot{\gamma}_{\text{wall}}\tau \lesssim 5$), we observe a plateau where the minimum value $w_b/w \sim 0.3$ is close to the experimental one [8]. This is due to lateral hydrodynamic diffusion [24] and the phenomenon is rather independent of the flow rate in this range of values.

Our simulations also predict a new phenomenon that was not experimentally observed on dilute suspensions: the jet fragmentation. If this instability is visually similar to the one observed in jets of falling passive particles [25] driven by gravity, the physical interpretation is totally different in our case since algae wear force dipoles while sedimenting passive particles wear single force (Stokeslet). Because they are aligned by light, the swimmers strongly interact with each other (in the simulations presented here, the volume fraction is ∼2.3%, i.e., corresponding to a semidilute case). By the mean of the forces created by the flagella and acting on the fluid (Fig. 1), swimmers create attractive flow field along their swimming direction and a repulsive flow field along their sides [26]. The attraction makes the jet unstable at larger times and a fragmentation in clusters happens [Fig. 2(c)]. Clusters merge together to form a large single one which then expands perpendicularly [Fig. 2(d)] to the channel owing to the side repulsion between pullers. Then, a self-focusing is observed again since the cluster size is comparable to the lateral size of the channel. Since clustering is driven by hydrodynamic interactions, it is only visible when suspension is concentrated enough (above ∼1%). In order to show the origin of this instability, we performed a simulation of a train of periodically arranged swimmers as described in Fig. 1, all oriented in one direction and suspended in a fluid at rest (Fig. 5).

The periodic structure is destabilized by the longitudinal attraction between pullers. Due to numerical noise, if two pullers become closer, they further form a pair and pairs then merge to form bigger clusters. This pairing does not depend on the period of the initial arrangement; the train is unconditionally unstable. Another approach that uses the Rotne-Prager-Green function for an infinite fluid [27,28] to calculate hydrodynamic interactions between swimmers gives the same results (not shown here). Oriented pullers always tend to cluster even when they are far apart. Therefore, in principle, the clustering should be experimentally observable even in dilute suspensions but on much larger timescales for which the phenomenon could be screened by other sources of noise (flow rate sensitivity, dispersion of size, swimming behaviors [12], and variability of phototactic properties among swimmers). Note that if body forces are reversed, pullers become pushers [10] and no instability is observed because of the longitudinal repulsion between pushers.

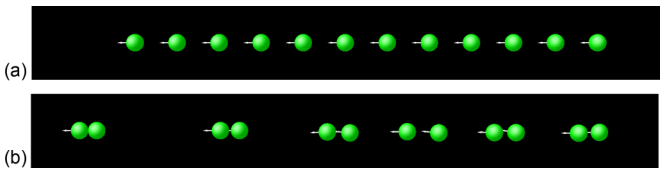

FIG. 5. (Color online) A train of pullers (as described in Fig. 1). (a) Initially, swimmers are regularly positioned and oriented in a fluid at rest in a channel (partial view). (b) A pairing appears due to hydrodynamic attractions between pullers.

IV. CONCLUSION AND FUTURE PROSPECTS

Our 3D simulations are able to reproduce the behavior of phototactic microswimmers in a channel flow at low Reynolds numbers. The self-focusing effect, the dynamics of the phenomenon, as well as its behavior as a function of the flow rate were studied for semidilute suspensions. We predict that the central jet of microswimmers once formed is unstable and a fragmentation in clusters occurs. The clustering is a collective behavior since it is due to attractive hydrodynamic interactions between oriented swimmers in the central jet. This is peculiar for pullers for which usually no collective motion is observed on such a time scale. This phenomenon should be experimentally observable for sufficiently concentrated suspensions. With this modeling, we hope to open new perspectives in the understanding of collective motions of active matter, including microalgae, which represent a rich domain of applications.

ACKNOWLEDGMENTS

C.M. acknowledges CNES (Centre National d'Etudes Spatiales) and ESA (European Space Agency). L.Q., S.R., and P.P. thank ANR MICMACSWIM. We all acknowledge the French-German University UFA (Université Franco Allemande) program.

[1] W. Durham, J. O. Kessler, and R. Stocker, Science **323**, 1067 (2009).
[2] A. Ghosh and P. Fischer, Nano Lett. **9**, 2243 (2009).
[3] A. Sokolov, R. E. Goldstein, F. I. Feldchtein, and I. S. Aranson, Phys. Rev. E **80**, 031903 (2009).
[4] T. V. Kasyap and D. L. Koch, Phys. Rev. Lett. **108**, 038101 (2012).
[5] A. Zöttl and H. Stark, Phys. Rev. Lett. **108**, 218104 (2012).
[6] J. Kessler, Nature **313**, 218 (1985).
[7] G. W. D. Stern and E. Harris, eds., *The Chlamydomonas Sourcebook* (Academic Press, New York, 2008).
[8] X. Garcia, S. Rafaï, and P. Peyla, Phys. Rev. Lett. **110**, 138106 (2013).
[9] J. Gachelin, A. Rousselet, A. Lindner, and E. Clement, New J. Phys. **16**, 025003 (2014).
[10] Pullers draw fluid from the front to the rear of their body, and push fluid out from the sides. Pushers repel fluid from the body at the rear, and draw fluid in to the sides [26].
[11] A. A. Evans, T. Ishikawa, T. Yamaguchi, and E. Lauga, Phys. Fluids **23**, 111702 (2011).
[12] M. Garcia, S. Berti, P. Peyla, and S. Rafaï, Phys. Rev. E **83**, 035301 (2011).

[13] V. Mehandia and P. R. Nott, J. Fluid Mech. **595**, 239 (2008).
[14] K. Drescher, R. E. Goldstein, N. Michel, M. Polin, and I. Tuval, Phys. Rev. Lett. **105**, 168101 (2010).
[15] S. Rafaï, L. Jibuti, and P. Peyla, Phys. Rev. Lett. **104**, 098102 (2010).
[16] H. Tanaka and T. Araki, Phys. Rev. Lett. **85**, 1338 (2000).
[17] P. Peyla, Europhys. **80**, 34001 (2007).
[18] Y. Davit and P. Peyla, Europhys. **83**, 64001 (2008).
[19] A. Sangani, A. Acrivos, and P. Peyla, Phys. Fluids **23**, 083302 (2011).
[20] L. Jibuti, S. Rafaï, and P. Peyla, J. Fluid Mech. **693**, 345 (2012).
[21] B. Maury, SIAM J. Numer. Anal. **47**, 1126 (2006).
[22] R. Peyret and T. D. Taylor, *Computational Methods for Fluid Flow* (Springer-Verlag, New York, 1963), p. 160.
[23] C. Pozrikidis, *Boundary Integral and Singularity Methods for Linearized Viscous Flow* (Cambridge University Press, Cambridge, 1992).
[24] In the experiments performed in the dilute regime [8], each alga can also diffuse on time scales of about 5–10 s [12]; this ingredient is not included in our model for sake of simplicity.
[25] M. Nicolas, Phys. Fluids **14**, 3570 (2002).
[26] E. Lauga and T. Powers, Reports Progr. Phys. **72**, 096601 (2009).
[27] J. Rotne and S. Prager, J. Chem. Phys. **50**, 4831 (1969).
[28] E. Wajnryb, A. Mizerski, A. Krzysztof, P. J. Zuk, and P. Szymczak, J. Fluid Mech. **731**, R3 (2013).